ACS APPLIED MATERIALS & INTERFACES

Letter

www.acsami.org

Quantitative Analysis and Optimization of Gravure Printed Metal Ink, Dielectric, and Organic Semiconductor Films

Stuart G. Higgins,[†,§] Francesca L. Boughey,[†,⊥,§] Russell Hills,[†] Joachim H. G. Steinke,[‡] Beinn V. O. Muir,*[,†,‡] and Alasdair J. Campbell[†]

[†]Department of Physics and Centre for Plastic Electronics and [‡]Department of Chemistry, Imperial College London, South Kensington Campus, London SW7 2AZ, United Kingdom

Supporting Information

ABSTRACT: Here we demonstrate the optimization of gravure printed metal ink, dielectric, and semiconductor formulations. We present a technique for nondestructively imaging printed films using a commercially available flatbed scanner, combined with image analysis to quantify print behavior. Print speed, cliché screen density, nip pressure, the orientation of print structures, and doctor blade extension were found to have a significant impact on the quality of printed films, as characterized by the spreading of printed structures and variation in print homogeneity. Organic semiconductor prints were observed to exhibit multiple periodic modulations, which are correlated to the underlying cell structure.

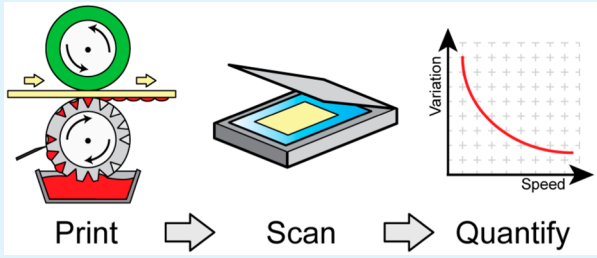

KEYWORDS: *gravure printing, nanoparticle metal ink, plastic electronics, image analysis, organic semiconductor, optical scanning, structure−property relationship, Fourier transform*

Organic electronics have been widely demonstrated as viable alternatives to silicon-based devices as organic field-effect transistors (OFETs), organic photovoltaics (OPVs), organic light-emitting diodes (OLEDs), and other structures.[1−3] By combining soluble metal inks, polymer dielectrics, and organic semiconductors with print technologies such as inkjet, flexographic, and gravure,[4,5] these devices have the potential to be manufactured inexpensively on mass, facilitating technological advances in areas such as lighting, displays, and much more.[6−9]

Gravure printing is of particular interest as it allows high throughput (>10 ms^{-1}) and large area (>1 m wide, and up to 1 km long) parallel manufacturing, with an inherent speed advantage over serial technologies.[5,10] However, to facilitate wider adoption of gravure printing, a greater understanding of the interaction between organic electronic materials and print parameters is required. This includes metal inks for the patterning of conductive electrodes;[11] dielectrics for capacitors, OFETs, and as device encapsulation;[12] and organic semiconductors for the design and operation of solid-state devices.[10,13]

The optimization of printed layers is challenging task, in part because of the complexity of the dynamic print process. In the case of intaglio methods such as gravure, printing is influenced by multiple parameters including print speed, nip pressure, doctor blade pressure, and cliché cell geometry. This problem is further compounded by the desire to print large-area structures, where even prints of modest dimensions (15 cm × 20 cm) are already too large for most lab-based microscopy techniques without destruction of the underlying sample. Here, we present how an affordable flatbed scanner can be combined with image processing techniques to quantitatively analyze and optimize gravure printed films. We demonstrate this technique by optimizing gravure printed silver nanoparticle ink, a commercially available dielectric ink, and a variety of organic semiconductor formulations. From this, we are able to infer underlying relationships between print quality and print parameters.

Figure 1 shows an illustration and photograph of the gravure printer used in this work, along with key parameters. The cliché is doctored with ink by the doctor blade, which then contacts the substrate in the nip region under pressure from the impression roller. Post print ink droplets may coalesce on the substrate, depending on solvent evaporation rate and relative interfacial energies. Spatial definition is achieved by selectively patterning the cliché with cells, typically by mechanical scribing or an electrochemical etching process.[14] The cell spacing (l_{cell}) is more commonly referred to by the reciprocal parameter screen density (l_{SD}), where $l_{SD} = l_{cell}^{-1}$, quoted in lines cm^{-1}.

For the work here, silver nanoparticle inks, a commercially available dielectric GSID 13447−1 (BASF),[12,15] and ink formulations of the organic semiconductors poly{[N,N′-bis(2-octyldodecyl)-naphthalene-1,4,5,8-bis(dicarboximide)-2,6-diyl]-*alt*-5,5′-(2,2′-bithiophene)} P(NDI2OD-T2) (ActivInk N2200, Polyera);[16] diketopyrrolopyrrole-thieno[3,2-*b*]thiophene (DPPT-TT, Flexink);[17] and an indacenodithiophene-benzo-

Received: December 2, 2014
Accepted: February 3, 2015
Published: February 3, 2015

DOI: 10.1021/am508316f
ACS Appl. Mater. Interfaces 2015, 7, 5045−5050

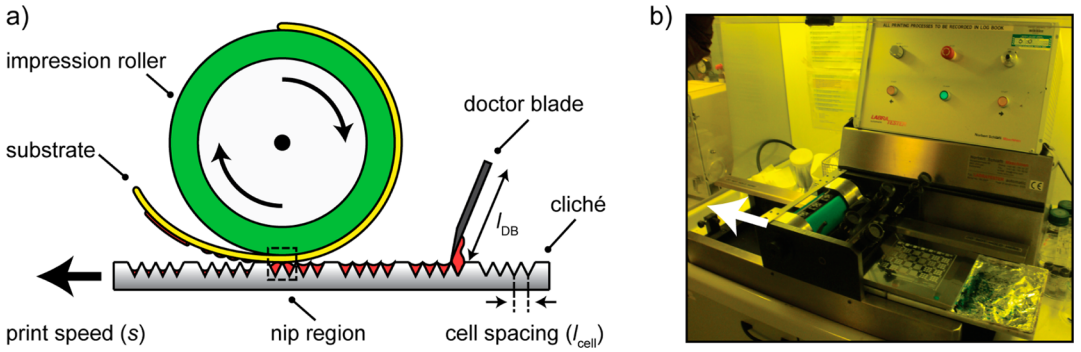

Figure 1. Gravure print process. (a) Illustration of gravure print mechanism, showing key parameters investigated here; (b) photograph of printer used.

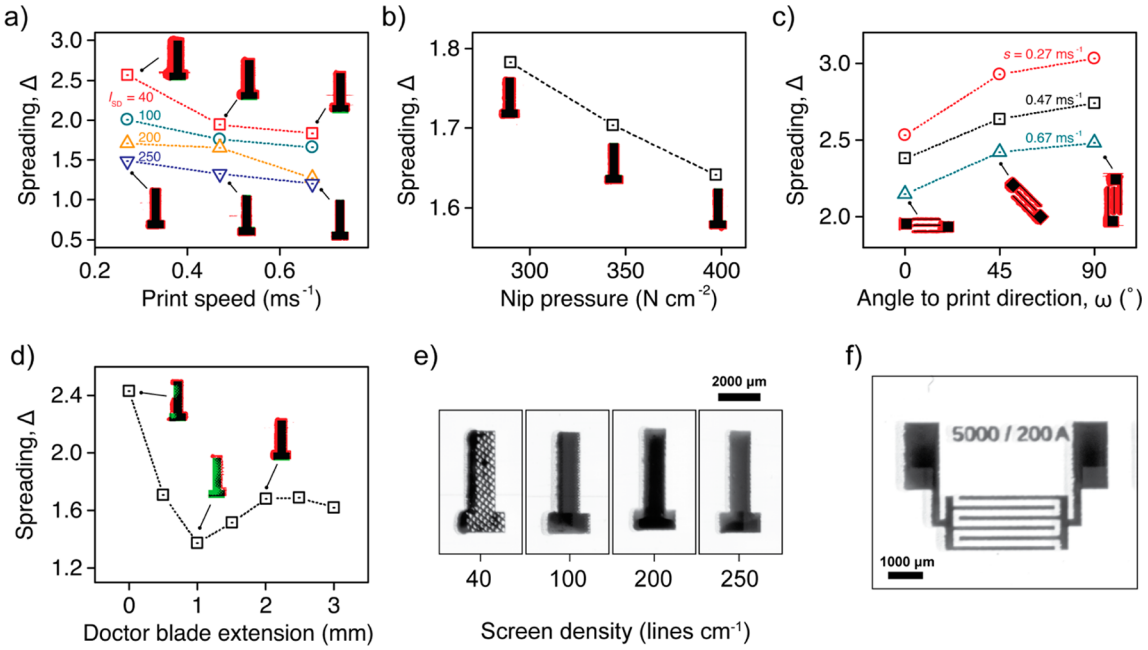

Figure 2. Impact of print parameters on the spreading of printed metal ink. (a) Print speed versus spreading for multiple screen densities. (b) Nip pressure versus spreading. (c) Orientation to print direction versus spreading. (d) Doctor blade extension versus spreading. (e) Scanned images of gate structure printed at varying screen densities. (f) Scanned image of optimized OFET source-drain structure. Each inset represents a single printed structure for illustration; the data points in a–d represent the average of 30, 120, 15, and 120 identical printed structures, respectively.

thiadiazole (C_{16}IDT-BT)[18] were prepared (see Supporting Information, Note S1, for further details). An electrochemically etched gravure cliché was used with a sheet fed gravure printer (Labratester, Norbert Schläfli Maschinen). The clichés contain features aligned at 0, 45, and 90° to the print direction, as well as seven different screen densities to facilitate optimization. Further details of the printer setup are discussed in the Supporting Information, Note S2.

Prints were scanned using a commercially available flatbed scanner; see the Supporting Information, Note S3, for details. A binary reference image was created from the cliché design data, representing a perfect print. The scanned images were transformed and registered to this reference, to provide equivalent scaling and accounting for differences in x- and y-calibration observed in the scanner. Images were processed using an image analysis tool (ImageJ, NIH)[19] and purpose-written analysis scripts (implemented in MATLAB 2013a, MathWorks). For metal inks, a constant binary luminance threshold of 0.95 was applied to all scanned images and each compared to the reference image. A composite image was generated, where black pixels indicates correct ink placement (Σx = total number of black pixels), red incorrect (y), and green missing ink (z). A parameter "spreading" was defined as $\Delta = (\Sigma x + \Sigma y)\Sigma x^{-1}$, where values $\Delta > 1$ indicate that the printed feature is larger than intended. For dielectric inks the mean (μ) and standard deviation (σ) of pixel intensity within each region of interest recorded, and the coefficient of variation ($c_v = \sigma/\mu$) calculated. For semiconductor inks each region of interest in the image was isolated, a fast Fourier transform performed, and the corresponding wavelength (λ) and the angle of modulation relative to the print direction (ω) extracted.

Figure 2 shows the optimization of gravure printed metal ink structures on plastic for various print parameters. This is also illustrated by the composite images shown in Figures 2a–d, (note: the intended design is effectively superimposed on top of the analyzed image).

Clear correlations are observed between print speed and ink spreading (Figure 2a). Faster print speeds were observed to reduce spreading, consistent with reduced ink transferred for a

DOI: 10.1021/am508316f
ACS Appl. Mater. Interfaces 2015, 7, 5045–5050

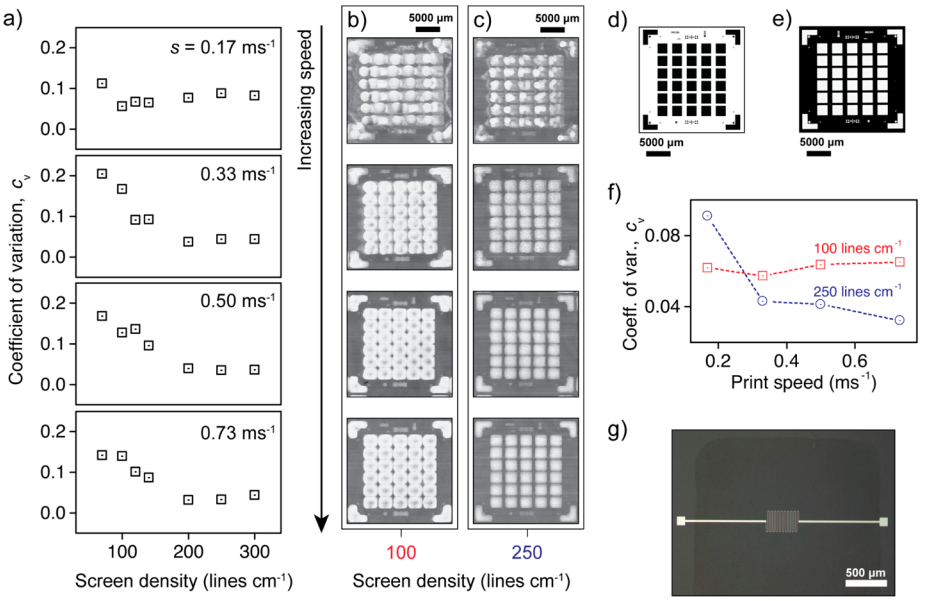

Figure 3. Impact of print speed and screen density on variation in printed films. (a) Screen density versus coefficient of variation for increasing print speed. (b) Scanned images of 5 × 6 arrays of printed dielectric at 100 lines cm^{-1} for the same increasing print speeds, also (c) at 200 lines cm^{-1}. (d) Cliché design data and (e) scanned image of corresponding cliché region for comparison. (f) Summary plot of analysis data for print speed versus coefficient of variation for b and c, where each data point represents 120 devices. (g) Optical micrograph of optimized printed dielectric pad on top of a photolithographically defined gate, on a flexible plastic substrate.

given print area.[20] Similarly increasing cliché screen density, which decreases the cell volume for a given area, was also observed to reduce spreading. Smaller cells have a reduced surface area to volume ratio, increasing the influence of ink adhesion to the cell walls, and reducing the relative proportion of ink transferred.[21,22]

Figure 2e shows a nominally identical structure printed with various line spacing. At l_{SD} = 40 lines cm^{-1} not only is greater spreading visible in the print, but also the cell structure of the cliché. Although common and often desirable in gravure halftone printing,[14] this effect must be minimized for printed electronics, as such structuring impacts the performance of the layer. This is a major difference between graphic arts and plastic electronic printing, demonstrating the need for a context-specific optimization approach.

Increasing the nip pressure was found to decrease spreading, as indicated in Figure 2b. The exact cause of this behavior is unclear, and interestingly contrasts with other reports. Nguyen et al. observed that the width of a printed silver nanoparticle line increased with nip pressure.[23] They attributed this to deformation of the plastic substrate under greater nip pressure, resulting in the filling of additional smaller cells at the edge of their main cliché cell structures. This mechanism is not possible here—these features are not present in our clichés because of the better line edge definition achieved by electrochemically etching the cells.[14] Instead, we suggest that increasing the nip pressure results in instability in the ink due to a greater pressure differential across the nip region.[24] This could potentially impede cell emptying, reducing ink transfer and hence spreading.

Ink spreading was observed to be dependent on print direction. Evenly spaced printed lines (inset in Figure 2c) illustrate how ink spreading was greater parallel to the print direction. Similar behavior has previously been attributed to the orientation of cell sidewalls, whereby rotating a structure can yield cells with narrower effective aspect ratios in the print direction, resulting in greater spreading.[25] The impact of such spreading is to short circuit adjacent device electrodes, and hence this effect must be taken into account when designing circuit layouts.

Figure 2d shows the impact of increasing the effective length of the doctor blade, l_{DB} (Figure 1) where l_{DB} = 0 mm represents the doctor blade just touching the cliché during printing. Increasing l_{DB} increases the pressure with which the doctor blade contacts the cliché. At low extensions, ink is not doctored but spread across the cliché, resulting in ink transfer from unpatterned areas of the cliché (as indicated by the high spreading value). With increasing extension, spreading decreases as ink is properly removed from these regions with a minima observed at l_{DB} = 1 mm. However, despite this, the low doctoring pressure also fails to fill the cliché cells, resulting in missing printed structures (as indicated by green pixels in the inset image). Increasing the blade extension to $l_{DB} \geq 2$ mm was observed to yield the required doctoring, and optimum results as shown in Figure 2f.

Variation in semitransparent dielectric films was also investigated as a function of print parameters. Figure 3a shows the impact of screen density and print speed upon film variation for a given dielectric ink formulation. Here the coefficient of variation quantifies the relative variation in pixel intensity for each region of interest. This represents a combination of both the average film thickness (and hence a change in the mean observed pixel intensity) as well as any inhomogeneity within each region, as indicated by the spread of data.

For print speeds $s > 0.17$ ms^{-1}, an inverse relationship is observed between screen density and the coefficient of variation, indicating that higher screen densities yield thinner films with less variation. At a print speed of $s = 0.17$ ms^{-1}, this relationship breaks down because of the high ink volume transferred to the substrate, causing the coalescence of adjacent structures, as shown in the corresponding array in Figure 3b.

DOI: 10.1021/am508316f
ACS Appl. Mater. Interfaces 2015, 7, 5045−5050

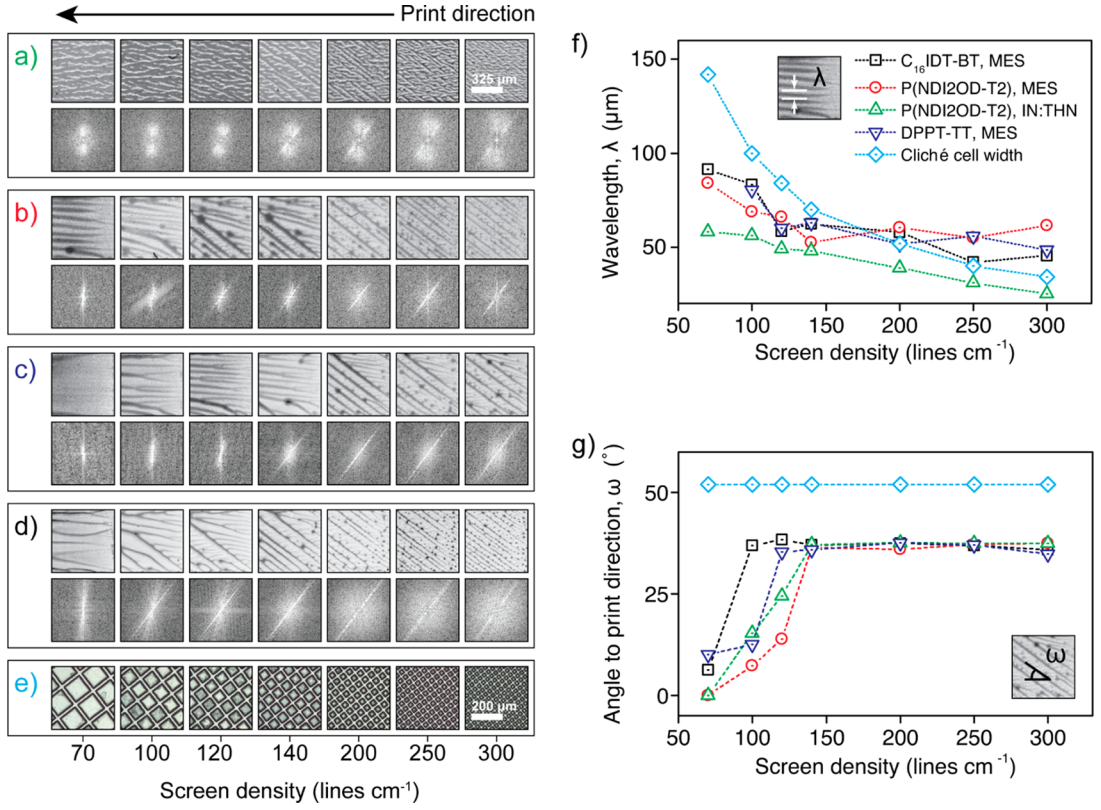

Figure 4. Impact of screen density on gravure printed semiconductor films, showing periodic modulation. Scanned images of printed semiconductor films and corresponding 2D frequency power spectra for: (a) P(NDI2OD-T2), 15 mg mL^{-1} in Indane:tetralin 1:1 v/v solvent blend; (b) P(NDI2OD-T2), 5 mg mL^{-1} in mesitylene; (c) DPPT-TT, 5 mg mL^{-1} in mesitylene; (d) C_{16}IDT-BT, 5 mg mL^{-1} in chlorobenzene. (e) Optical micrographs of corresponding cliché regions (note a difference in scales due to the limited field of view of the microscope). (f) Summary of screen density versus modulation wavelength and (g) angle of modulation to print direction versus screen density, extracted from images.

To understand the impact of this behavior in a manufacturing context, we made prints of 5 × 6 arrays of printed dielectric squares at both 100 and 200 lines cm^{-1}, designed for the manufacture of OFETs. The combined numerical results are summarized in Figure 3f. Behavior at 100 lines cm^{-1} is inconsistent because of a high volume of ink transferred; however, at 200 lines cm^{-1}, a clear reduction in variation is observed with increasing speed and screen density, consistent with the reduction in spreading observed for the metal ink above. Kang et al. observed similar behavior for gravure printed metal inks and the dielectric poly(4-vinylphenol),[11] where better pattern definition and less variation occurs when viscous forces dominate the print transfer process, rather than the relative interfacial energy of ink and substrate. This agrees well with the uncontrolled wetting/spreading behavior observed at s = 0.17 ms^{-1}.

Overall, a print speed of s = 0.73 ms^{-1} and a screen density of l_{SD} = 200 lines cm^{-1} yielded arrays with minimal variation and spreading, important for reducing device-to-device differences in the layer capacitance.[12,26] The outcome of the optimization process is shown in Figure 3g, with an optical micrograph of the optimized dielectric layer printed on top of a photolithographically patterned transistor gate. The film is printed without pinhole defects, and with good separation of dielectric between adjacent devices, allowing for interconnects to be patterned between layers.

Figure 4 shows the impact of screen density on printed film variation for various semiconductor ink formulations. Unlike dielectrics, which are generally viscous because of the presence of high-molecular-weight polymer modifiers,[12,27] state-of-the-art organic semiconductor formulations are normally constrained by the expense of producing large quantities of high concentration inks.[28] Consequently, it was observed that lower viscosity semiconductor formulations were more susceptible to high film variation than either the printed metal ink or dielectric presented above.

At low screen densities, periodic film modulation was observed parallel to the print direction. Figure 4f shows how the modulation wavelength (λ) decreases as a function of increasing screen density, consistent with the corresponding decrease in cell width and spacing. For low viscosity inks, this modulation can occur as a consequence of two immiscible fluids (in this case ink and air) mixing during the ink transfer process, referred to as "viscous fingering".[29,30] Of particular interest, however, is the emergence of a secondary modulation mode at higher screen densities, as seen by the diagonal lines in the scanned images. Here we define ω as the angle of this modulation relative to the print direction. Figure 4g shows screen density versus ω as a function of different semiconductor formulations. All films tend to the same value ($\omega \approx 35°$); however, the onset is ink-dependent, suggesting that the viscosity of each formulation impacts this behavior. This was confirmed by analyzing prints of the same semiconductor, but in a less viscous ink formulation (compare Figure 4a, b).

To understand the origin of the secondary modulation, we made optical micrographs of each cliché cell structure, as shown in Figure 4e. For all screen densities the cells are orientated at a constant angle of $\omega \approx 52°$ to the print direction, indicating that

DOI: 10.1021/am508316f
ACS Appl. Mater. Interfaces 2015, 7, 5045−5050

cell geometry is the probable cause of film modulation. The dependence on screen density seen in Figure 4g suggests that this effect is dominant only for higher screen densities, which is in contrast to the general trend observed above (namely that higher screen density is preferable). It is important to consider the impact of this modulation while designing cliché geometries that are to be used with multiple material systems.

In conclusion, our technique has demonstrated that print speed and cliché screen density have a significant impact on the morphology of solution-processable materials for organic electronics. Spreading of silver nanoparticle inks is reduced at higher print speeds and, in contrast to previous results, also by increased impression pressure, most likely as a result of incomplete ink transfer due to ink instabilities in the nip region. By reducing variation and spreading in printed dielectric films, we have demonstrated the optimized printing of large arrays of dielectric pads. Periodic film modulations were observed both parallel and at an angle to the print direction in low concentration semiconductor formulations. This was observed to be both formulation dependent, as well as related to the underlying cliché structure. These findings imply that our analysis techniques are a powerful tool for analyzing printed films, and for providing insight into appropriate print and design parameters. Traditional graphics arts approaches to cliché design are unlikely to be sufficient to accommodate the demands for printed electronic films, namely homogeneous, noncontiguous structures.

■ ASSOCIATED CONTENT

Supporting Information

Additional details about the ink formulations, printer setup, and scan parameters. This material is available free of charge via the Internet at http://pubs.acs.org.

■ AUTHOR INFORMATION

Corresponding Author

*E-mail: bmuir@imperial.ac.uk.

Present Address

[⊥]F.L.B. is currently at Department of Materials Science & Metallurgy, University of Cambridge, 27 Charles Babbage Road, Cambridge, CB3 OFS, United Kingdom

Author Contributions

[§]The authors S.G.H. and F.L.B. contributed equally. S.G.H. performed dielectric and semiconductor printing, created the analysis technique and scripts, performed analysis, and wrote the manuscript. F.L.B. performed metal ink printing, wrote analysis scripts, and performed analysis on metal inks. R.H. performed metal ink printing and performed analysis. B.V.O.M. performed metal ink printing, supervised, and set the scientific aims. J.H.G.S. and A.J.C. supervised and set the scientific aims.

Notes

The authors declare no competing financial interest.

■ ACKNOWLEDGMENTS

This work has been supported by the European Commission's 7th Framework Programme (FP7/2007-2013) under grant agreement 247978 (POLARIC). S.G.H. was supported by the Engineering and Physical Sciences Research Council (EPSRC) under grant number EP/P505550/1.

■ REFERENCES

(1) Horowitz, G. Organic Field-Effect Transistors. *Adv. Mater.* **1998**, *10*, 365−377.

(2) Li, G.; Zhu, R.; Yang, Y. Polymer Solar Cells. *Nat. Photonics* **2012**, *6*, 153−161.

(3) Wolk, M. B. In *Organic Electroluminescence*; Kafafi, Z., Ed.; Taylor & Francis Group: Baca Raton, FL, 2005; Chapter 7, pp 307−353.

(4) Kang, B.; Lee, W. H.; Cho, K. Recent Advances in Organic Transistor Printing Processes. *ACS Appl. Mater. Interfaces* **2013**, *5*, 2302−2315.

(5) Søndergaard, R. R.; Hösel, M.; Krebs, F. C. Roll-to-Roll Fabrication of Large Area Functional Organic Materials. *J. Polym. Sci., Part B: Polym. Phys.* **2013**, *51*, 16−34.

(6) Baeg, K.-J.; Caironi, M.; Noh, Y.-Y. Toward Printed Integrated Circuits Based on Unipolar or Ambipolar Polymer Semiconductors. *Adv. Mater.* **2013**, *25*, 4210−4244.

(7) Kopola, P.; Tuomikoski, M.; Suhonen, R.; Maaninen, A. Gravure Printed Organic Light Emitting Diodes for Lighting Applications. *Thin Solid Films* **2009**, *517*, 5757−5762.

(8) Lee, T.-M.; Noh, J.-H.; Kim, C. H.; Jo, J.; Kim, D.-S. Development of a Gravure Offset Printing System for the Printing Electrodes of Flat Panel Display. *Thin Solid Films* **2010**, *518*, 3355−3359.

(9) Forrest, S. R. The Path to Ubiquitous and Low-Cost Organic Electronic Appliances on Plastic. *Nature* **2004**, *428*, 911−918.

(10) Voigt, M. M.; Guite, A.; Chung, D.-Y.; Khan, R. U. A.; Campbell, A. J.; Bradley, D. D. C.; Meng, F.; Steinke, J. H. G.; Tierney, S.; McCulloch, I.; Penxten, H.; Lutsen, L.; Douherent, O.; Manca, J.; Brokmann, U.; Sönnichsen, K.; Hülsenberg, D.; Bock, W.; Barron, C.; Blanckaert, N.; Springer, S.; Grupp, J.; Mosley, A. Polymer Field-Effect Transistors Fabricated by the Sequential Gravure Printing of Polythiophene, Two Insulator Layers, and a Metal Ink Gate. *Adv. Funct. Mater.* **2010**, *20*, 239−246.

(11) Kang, H.; Kitsomboonloha, R.; Jang, J.; Subramanian, V. High-Performance Printed Transistors Realized Using Femtoliter Gravure-Printed Sub-10 Mm Metallic Nanoparticle Patterns and Highly Uniform Polymer Dielectric and Semiconductor Layers. *Adv. Mater.* **2012**, *24*, 3065−3069.

(12) Vaklev, N. L.; Müller, R.; Muir, B. V. O.; James, D. T.; Pretot, R.; van der Schaaf, P.; Genoe, J.; Kim, J.-S.; Steinke, J. H. G.; Campbell, A. J. High-Performance Flexible Bottom-Gate Organic Field-Effect Transistors with Gravure Printed Thin Organic Dielectric. *Adv. Mater. Interfaces* **2014**, *1*, 1300123.

(13) Chung, D.; Huang, J.; Bradley, D. High Performance, Flexible Polymer Light-Emitting Diodes (PLEDs) with Gravure Contact Printed Hole Injection and Light Emitting Layers. *Org. Electron.* **2010**, *11*, 1088−1095.

(14) Kipphan, H. *Handbook of Print Media*, 1st ed; Springer-Verlag: Heidelberg, Germany, 2001.

(15) Kastler, M.; Köhler, S. Crosslinkable Dielectrics and Methods of Preparation and Use Thereof. U.S. Patent 8,853,820, Oct 7, 2014.

(16) Yan, H.; Chen, Z.; Zheng, Y.; Newman, C.; Quinn, J. R.; Dötz, F.; Kastler, M.; Facchetti, A. A High-Mobility Electron-Transporting Polymer for Printed Transistors. *Nature* **2009**, *457*, 679−686.

(17) Chen, Z.; Lee, M. J.; Shahid Ashraf, R.; Gu, Y.; Albert-Seifried, S.; Meedom Nielsen, M.; Schroeder, B.; Anthopoulos, T. D.; Heeney, M.; McCulloch, I.; Sirringhaus, H. High-Performance Ambipolar Diketopyrrolopyrrole-thieno[3,2-B]thiophene Copolymer Field-Effect Transistors with Balanced Hole and Electron Mobilities. *Adv. Mater.* **2012**, *24*, 647−652.

(18) Zhang, W.; Smith, J.; Watkins, S. E.; Gysel, R.; McGehee, M.; Salleo, A.; Kirkpatrick, J.; Ashraf, S.; Anthopoulos, T.; Heeney, M.; McCulloch, I. Indacenodithiophene Semiconducting Polymers for High-Performance, Air-Stable Transistors. *J. Am. Chem. Soc.* **2010**, *132*, 11437−11439.

(19) Schneider, C. a; Rasband, W. S.; Eliceiri, K. W. NIH Image to ImageJ: 25 Years of Image Analysis. *Nat. Methods* **2012**, *9*, 671−675.

DOI: 10.1021/am508316f
ACS Appl. Mater. Interfaces 2015, 7, 5045−5050

(20) Elsayad, S.; Morsy, F.; El-Sherbiny, S.; Abdou, E. Some Factors Affecting Ink Transfer in Gravure Printing. *Pigm, Resin Technol.* **2002**, *31*, 234−240.
(21) Yin, X.; Kumar, S. Flow Visualization of the Liquid Emptying Process in Scaled-up Gravure Grooves and Cells. *Chem. Eng. Sci.* **2006**, *61*, 1146−1156.
(22) Sung, D.; de la Fuente Vornbrock, A.; Subramanian, V. Scaling and Optimization of Gravure-Printed Silver Nanoparticle Lines for Printed Electronics. *IEEE Trans. Compon., Packag., Technol.* **2010**, *33*, 105−114.
(23) Nguyen, H. A. D.; Lee, J.; Kim, C. H.; Shin, K.-H.; Lee, D. An Approach for Controlling Printed Line-Width in High Resolution Roll-to-Roll Gravure Printing. *J. Micromech. Microeng.* **2013**, *23*, 095010.
(24) Bohan, M. F. J.; Lim, C. H.; Korochkina, T. V.; Claypole, T. C.; Gethin, D. T.; Roylance, B. J. An Investigation of the Hydrodynamic and Mechanical Behaviour of a Soft Nip Rolling Contact. *Proc. Inst. Mech. Eng., Part J.* **1997**, *211*, 37−49.
(25) Lee, T.-M.; Lee, S.-H.; Noh, J.-H.; Kim, D.-S.; Chun, S. The Effect of Shear Force on Ink Transfer in Gravure Offset Printing. *J. Micromech. Microeng.* **2010**, *20*, 125026.
(26) Hambsch, M.; Reuter, K.; Stanel, M.; Schmidt, G.; Kempa, H.; Fügmann, U.; Hahn, U.; Hübler, A. C. Uniformity of Fully Gravure Printed Organic Field-Effect Transistors. *Mater. Sci. Eng., B* **2010**, *170*, 93−98.
(27) Maliakal, A. In *Organic Field-Effect Transistors*; Bao, Z., Locklin, J., Eds.; Taylor & Francis Group: Boca Raton, FL, 2007; Chapter 3, pp 229−251.
(28) Berggren, M.; Nilsson, D.; Robinson, N. D. Organic Materials for Printed Electronics. *Nat. Mater.* **2007**, *6*, 3−5.
(29) Hernandez-Sosa, G.; Bornemann, N.; Ringle, I.; Agari, M.; Dörsam, E.; Mechau, N.; Lemmer, U. Rheological and Drying Considerations for Uniformly Gravure-Printed Layers: Towards Large-Area Flexible Organic Light-Emitting Diodes. *Adv. Funct. Mater.* **2013**, *23*, 3164−3171.
(30) Reuter, K.; Kempa, H.; Brandt, N.; Bartzsch, M.; Huebler, A. C. Influence of Process Parameters on the Electrical Properties of Offset Printed Conductive Polymer Layers. *Prog. Org. Coat.* **2007**, *58*, 312−315.

DOI: 10.1021/am508316f
ACS Appl. Mater. Interfaces 2015, 7, 5045−5050